Pathway dependence of ecosystem responses in China to 1.5°C global warming

Xu Yue[1], Hong Liao[1], Huijun Wang[2], Tianyi Zhang[3], Nadine Unger[4], Stephen Sitch[4], Zhaozhong Feng[1] and Jia Yang[5]

[1] Jiangsu Key Laboratory of Atmospheric Environment Monitoring and Pollution Control, Collaborative Innovation Center of Atmospheric Environment and Equipment Technology, School of Environmental Science and Engineering, Nanjing University of Information Science & Technology (NUIST), Nanjing, 210044, China
[2] Ministry of Education Key Laboratory of Meteorological Disaster, Joint International Research Laboratory of Climate and Environment Change, Collaborative Innovation Center on Forecast and Evaluation of Meteorological Disasters, NUIST, Nanjing, 210044, China
[3] State Key Laboratory of Atmospheric Boundary Layer Physics and Atmospheric Chemistry, Institute of Atmospheric Physics, Chinese Academy of Sciences, Beijing, 100029, China
[4] College of Engineering, Mathematics and Physical Sciences, University of Exeter, Exeter, EX4 4QE, UK
[5] Department of Forestry, Mississippi State University, Mississippi State, MS, 39762, US

Email: yuexu@nuist.edu.cn and hongliao@nuist.edu.cn

Abstract

China is currently the world's largest emitter of both CO_2 and short-lived air pollutants. The ecosystems in China help mitigate a part of its carbon emissions, but are subject to perturbations in CO_2, climate, and air pollution. Here, we use a dynamic vegetation model and data from three model inter-comparison projects to examine ecosystem responses in China under different emission pathways towards the 1.5°C warming target set by the Paris Agreement. At 1.5°C warming, gross primary productivity (GPP) increases by 15.5±5.4 % in a stabilized pathway and 11.9±4.4 % in a transient pathway. CO_2 fertilization is the dominant driver of GPP enhancement and climate change is the main source of uncertainties. However, differences in ozone and aerosols explain the GPP differences between pathways at 1.5°C warming. Although the land carbon sink is weakened by 17.4±19.6 % in the stabilized pathway, the ecosystems mitigate 10.6±1.4% of national emissions in the stabilized pathway, more efficient than the fraction of 6.3±0.8% in the transient pathway. To achieve the 1.5°C warming target, our analysis suggests a higher allowable carbon budget for China under a stabilized pathway with reduced emissions in both CO_2 and air pollutants.

Keywords: Ecosystems, climate change, 1.5°C warming, emission pathway, ozone vegetation damage

1 Introduction

The past decade has seen record-breaking warming largely related to anthropogenic greenhouse gas emissions (Mann et al., 2017). This warming trend presents a challenge to achieve the temperature control target of 1.5°C above the pre-industrial (PI) level set by the 2015 Paris climate agreement. Many studies have shown that a conservative warming such as 1.5°C is necessary to limit climatic extremes (Nangombe et al., 2018), avoid heat-related mortality (Mitchell et al., 2018), reduce economic loss(Burke et al., 2018), and alleviate ecosystem risks (Warszawski et al., 2013) compared to stronger anthropogenic warming. To achieve this target, each country must aim to control its greenhouse gas emissions. A full understanding of regional ecosystem response to the changing climate and environmental stress is essential to reduce uncertainties in allowable carbon budget estimates at 1.5°C (Mengis et al., 2018). China is covered with a wide range of terrestrial biomes (Fang et al., 2012). While China's ecosystem response to possible future climate has been explored (Wu et al., 2009;He et al., 2017;Dai et al., 2016), impacts on the regional carbon budget of differing pathways to the 1.5°C target are not known.

There are two distinct pathways to the 1.5°C global warming. One is a fast process in which global temperature passes 1.5°C and continues to increase (scenarios assuming high CO_2 emissions and no climate mitigation) while the other is a stabilized process with an equilibrium warming right below 1.5°C and last for decades before the end of 21st century (scenarios including climate mitigation) (James et al., 2017). The stabilized pathway is the one proposed by the 2015 Paris agreement. However, the unprecedented warming in 2016 results in an increase of global average temperature by 1.1°C above PI (https://public.wmo.int), suggesting that the 1.5°C limit can be broken in a near future under a transient pathway (Henley and King, 2017). A few studies have compared allowable carbon budgets between these two pathways (Collins et al., 2018;Millar et al., 2017), but none has estimated the mitigation potential of regional ecosystems with joint impacts of changes in climate, CO_2, and air pollution under different pathways.

Here, we apply the Yale Interactive terrestrial Biosphere Model (YIBs) (Yue and Unger, 2015;Yue and Unger, 2018) to investigate the response of terrestrial ecosystem productivity in China to both stabilized and transient global warming of 1.5°C relative to PI period. We focus on the changes of gross primary productivity (GPP) and net ecosystem exchange (NEE). GPP represents the total canopy photosynthesis through gross carbon assimilation. NEE is the residue after subtraction of GPP from ecosystem (plant plus soil) respiration (Reco – GPP), indicating the net carbon sink from land to atmosphere. The larger the GPP values, the stronger carbon assimilation by ecosystems. In contrast, the more negative the NEE, the stronger carbon sink of land. The YIBs model is driven with meteorology from an ensemble of climate models in Climate Model Intercomparison Project Phase 5 (CMIP5). The stabilized global warming pathway is represented by the RCP2.6 low emissions scenario that yields an equilibrium change in Global Mean Temperature (ΔGMT) of 1.49°C by 2050-2070 with selected climate models (Fig. S1). The transient pathway is represented by RCP8.5 high emission scenario in which ΔGMT grows rapidly and realizes a transient 1.5°C around the year 2021-2041. We select the present-day period of 1995-2015 as a reference.

2 Methods

2.1 Datasets

2.1.1 CMIP5 data

We use both daily and monthly meteorology predicted by CMIP5 models (https://cmip.llnl.gov/). The daily data are used as input for YIBs model. In total, we select 15 climate models (Table S1) with all available daily meteorology, including surface air temperature, precipitation, specific humidity, surface downward shortwave radiation, surface pressure, and surface wind speed, for historical and two future scenarios (RCP2.6 and RCP8.5). These two scenarios assume distinct emission pathways of both CO_2 and air pollutants, with the RCP2.6 scenario projecting much lower CO_2 and pollution concentrations than RCP8.5. Simulated annual GMT is

smoothed with a 21-year window to remove decadal variations. The ensemble changes of GMT relative to PI period (1861-1900) from two scenarios are examined (Fig. S1a). The low emission scenario RCP2.6 yields an equilibrium ΔGMT of 1.85°C by 2100. We remove 8 climate models predicting stabilized ΔGMT higher than 1.85°C by the end of century. The 7 remaining models yield an ensemble warming close to 1.5°C (1.49°C for 2050-2070, Fig. S1b). Meanwhile, ΔGMT in the high emission scenario RCP8.5 grows fast and realizes a transient 1.5°C warming around the year 2021-2041. Daily meteorology from 7 selected models (Table S1) are then interpolated to the uniform 1°×1° resolution and used to drive YIBs model to simulate terrestrial carbon fluxes in China for 1850-2100. Due to the large data storage, we retain only the domain of [15-60ºN, 60-150ºE] covering China territory. We bias correct modeled meteorology with WFDEI (WATCH Forcing Data methodology applied to ERA-Interim reanalysis) data (Weedon et al., 2014):

$$V_d^s = V_d \times S_w / S_m \quad (1)$$

Here V_d is the original daily variables and V_d^s is the scaled value. S_w is the 2-dimensional WFDEI value averaged for 1980-2004 and S_m is the modeled values averaged at the same period. In this case, the average climate from each individual model matches observations at present day; meanwhile, climate variability from models are retained to estimate uncertainties in carbon fluxes.

2.1.2 TRENDY-v6 data

We acquire the global GPP and NEE datasets from 1901 to 2016 simulated by 14 Dynamic Global Vegetation Models (DGVMs) participating in TRENDY project (Table S2). All DGVMs are implemented following the same simulation protocol and driven by consistent input datasets, including CRU-NCEP climate data, atmospheric CO_2 concentrations, but fixed present-day land use (Le Quere et al., 2018).

2.1.3 ACCMIP O_3 data

We use monthly output of surface O_3 concentrations from 12 models joining the Atmospheric Chemistry and Climate Model Intercomparison Project (ACCMIP, Lamarque et al., 2013) (Table S3). The ACCMIP models have a wide range of horizontal and vertical resolutions, natural emissions, chemistry schemes, and interaction with radiation and clouds. However, these models apply the same anthropogenic and biomass burning emissions specified for CMIP5 RCP scenarios (e.g., RCP2.6 or RCP8.5), though different models perform simulations at different time slices. Here, we use surface O_3 and interpolate original output to 1°×1° resolution. We fill the temporal gaps between two adjacent time slices using a linear fitting approach. In this way, we derive the monthly O_3 from 1850 to 2100 for each model and their ensemble average at each grid point.

2.1.4 Diffuse radiation data

The original CMIP5 archive does not provide diffuse component of shortwave radiation. Here, we use empirical relations between total and diffuse radiation from 11 studies to calculate hourly diffuse radiation (Table S4). The diffuse fraction k_d in all equations depends on clearness index k_t, which is defined as the ratio between global solar radiation I_t and extra-terrestrial solar radiation I_0 (Ghosh et al., 2017):

$$k_t = I_t / I_0 \quad (2)$$

$$I_0 = I_{sc}\left[1 + 0.033cos\left(\frac{360N}{365}\right)\right]cos\varphi \quad (3)$$

Here I_{sc} = 1367 W m^{-2} is solar constant, N is Julian day of the year, and φ is solar zenith. The empirical equations are evaluated using hourly total and diffuse radiation from Modern-Era Retrospective Analysis for Research and Applications (MERRA) (Rienecker et al., 2011) during 2008-2012. For each grid in China, we calculate hourly diffuse radiation (D_c) using MERRA total radiation and compare it with the standard output (D_m). Statistical metrics including correlation, normalized mean bias (NMB), and normalized root mean square error (NRMSE) are used to evaluate the performance of empirical equations:

$$\mathrm{NMB} = (\overline{D_c} - \overline{D_m})/\overline{D_m} \quad (4)$$

$$\mathrm{NRMSE} = \sqrt{\sum \frac{(D_c - D_m)^2}{n}} \Big/ \overline{D_m} \quad (5)$$

Here $\overline{D_c}$ and $\overline{D_m}$ are mean values of calculated and MERRA diffuse radiation, respectively. The evaluation is performed month by month for 2008-2012 and *n* is the number of daytime samples (grids with total radiation > 5 W m^{-2}). The value of *n* varies from month to month with a minimum of 540,000 in December 2010. Evaluation shows the empirical model M01 (Lam and Li, 1996) yields the highest correlation and the lowest NRMSE (Fig. S2). As a result, we use M01 model to derive diffuse radiation from CMIP5 models.

2.2 Model

We apply the YIBs model (Yue and Unger, 2015;Yue et al., 2017) to simulate historical and future (1850-2100) ecosystem productivity. The YIBs model dynamically calculates LAI and tree height based on carbon assimilation and allocation. Leaf-level photosynthesis is calculated hourly using the well-established Farquhar et al. (1980) scheme and is upscaled to canopy level by the separation of sunlit and shading leaves (Spitters, 1986). Sunlit leaves can receive both direct and diffuse radiation, while shading leaves receive only the diffuse component (Yue and Unger, 2017). The assimilated carbon is in part used for maintenance and growth respiration, and the rest is allocated among leaf, stem, and root for plant growth (Clark et al., 2011). Soil respiration is calculated as the loss of carbon flows among 12 soil carbon pools (Schaefer et al., 2008). The YIBs model considers 9 plant functional types (PFTs) including evergreen needleleaf forest (ENF), deciduous broadleaf forest (DBF), evergreen broadleaf forest (EBF), shrubland, tundra, C3 grassland, C4 grassland, C3 cropland, and C4 cropland. The land cover is prescribed based on satellite retrievals from the Moderate Resolution Imaging Spectroradiometer (MODIS) (Hansen et al., 2003) and the Advanced Very High Resolution Radiometer (AVHRR) (Defries et al., 2000). For this study, we fix the land cover to isolate impacts of CO_2 and climatic changes. Other studies also show only moderate changes in vegetation fraction and composition at a low warming level (Warszawski et al., 2013). The YIBs model can be

applied at the site, regional, and global scales. The site-level model has been evaluated with measured carbon fluxes from 145 FLUXNET sites (Yue and Unger, 2015). For this study, all simulations are performed at the 1°×1° resolution over China. During the period of 1982-2011, YIBs predicts an average GPP of 7.17 Pg C yr^{-1} in China (Fig. S3), close to the 7.25 Pg C yr^{-1} estimated in the benchmark product (Jung et al., 2009).

YIBs model calculates O_3 damage to plant photosynthesis using a flux-based parameterization (Sitch et al., 2007). The inhibition rate of GPP is dependent on both ambient O_3 concentrations and stomatal conductance. Compared to meta-analyses of hundreds of data from China (Table S5) and the world (Yue and Unger, 2018), the scheme shows good performance in estimating GPP responses to O_3 for DBF, EBF, C3 and C4 herbs (Fig. S4). The predicted O_3 damaging effects to ENF might be underestimated. The YIBs model separates the effects of diffuse and direct light on plant photosynthesis (Spitters, 1986). Simulated GPP responses to direct and diffuse radiation show good agreement with observations at 24 global flux tower sites from FLUXNET network (Yue and Unger, 2018). In general, diffuse radiation is more efficient to enhance canopy photosynthesis compared to the same level of direct radiation.

2.3 Simulations

We perform two main groups of simulations, one for RCP2.6 and the other for RCP8.5. For each group, 7 sub-groups are designed with varied climatic or CO_2 forcings (Table S6). In each sub-group, separate runs are conducted for the YIBs model driven with climate variables from 7 selected CMIP5 models (Table S1), making a total of 98 runs. A baseline group (HIST_2000) is performed with fixed meteorology and CO_2 after the year 2000. Another four sub-group simulations are performed to quantify O_3 effects on photosynthesis (Table S7). These simulations are driven with both CMIP5 meteorology and monthly O_3 concentrations from an ensemble of 12 ACCMIP models. The runs are distinguished with different O_3 damaging sensitivity (high or low) and scenario projections (RCP2.6 or RCP8.5). Monthly O_3 concentrations are downscaled to hourly

step using the diurnal cycle simulated by a chemistry-climate model NASA ModelE2 (Schmidt et al., 2014). The O_3-affected GPP or NEE are calculated as the average of simulations with low and high sensitivities.

For each run, a 251-year simulation is performed with historical climate for 1850-2000 and future climate for 2001-2100. For simulations driven with meteorology from the same climate model, all sensitivity tests apply the same climate forcing during historical period but utilize varied forcings after the year 2000. For example, RCP26_CO2 is identical to RCP26_MET for the period of 1850-2000. However, after the year 2000, the former runs fix climatic conditions at the year 2000 but allow changes in CO_2 concentrations year by year for 2001-2100 following the pathway projection, while the latter fix CO_2 level at the year 2000 but continue to use day-to-day meteorology after 2000. For all simulations, we initialize vegetation and soil carbon pools in the YIBs model with a 200-year spin up by recycling meteorology at the year of 1850. Contributions of individual factors are calculated as the differences between sensitivity and baseline group (e.g., RCP26_CO2 – HIST_2000 for CO_2 fertilization in RCP2.6 scenario).

The main focus of this study is to quantify how the differences of anthropogenic emissions, including both CO_2 and air pollution which are usually associated, will cause different responses in land carbon budget to the same global warming target. Especially, the role of air pollution on land carbon cycle has always been ignored. The assumptions of land use can be quite uncertain between future pathways (Stehfest et al., 2019), and these assumptions are not necessarily associated with CO_2 and air pollution emissions. As a result, for this study, we consider fixed land cover in all simulations. We do not consider ecosystem-climate interactions as in the earlier studies (e.g., Yue et al., 2017), so as to take advantage of climate projections from multiple models.

3 Results

3.1 Changes of atmospheric compositions and radiation

The ensemble concentrations of ACCMIP O_3 show good agreement with ground-based observations from 1580 sites in China (Fig. 1). The spatial correlation is R=0.80 (p < 0.01) between observations and the ensemble O_3 concentrations ([O_3]), though the latter is higher by 25% (Figs. 1a-1c). Such overestimation is likely attributed to the high [O_3] at night in the models, because the evaluation of maximum daily 8-hour average (MDA8) [O_3], which mainly occurs in the daytime, shows more reasonable predictions with a lower bias of 10% (Figs. 1d-1f). Since the O_3 vegetation damage in general occurs in the daytime, when both plant photosynthesis and [O_3] are at high levels, the ACCMIP [O_3] is good to be used as input for YIBs model to derive long-term O_3 inhibition effects on ecosystem productivity.

The ensemble radiation from CMIP5 models matches observations at 106 sites in China (Fig. 2). For total shortwave radiation, the model prediction shows high values in the West and low values in the Southeast, consistent with observations for a correlation coefficient of R = 0.79 (p < 0.01) and a mean bias of 8.9%. The derived diffuse radiation is highest in the Southeast, where the total radiation is lowest. Observed diffuse radiation is available only at 17 sites. Compared to these sites, predictions show reasonable spatial distribution with a correlation of R = 0.65 (p < 0.01) and a low bias of 7.1%. Both the total radiation and derived diffuse radiation are used as input for YIBs model to estimate GPP responses to joint changes in direct and diffuse radiation caused by aerosol removal.

Atmospheric compositions and radiation show varied changes in different scenarios. The GMT changes mainly follow those in CO_2 concentrations, which show fast growth in RCP8.5 but slow changes in RCP2.6 (Fig. 3a). The latter assumes a large reduction of carbon emissions globally after the year 2020 (Meinshausen et al., 2011). Global CO_2 levels reduce slightly after the year 2030 in RCP2.6, while GMT continues growing until 2050 due to air-sea interactions (Solomon et al., 2009). As a low emission scenario, RCP2.6 experiences a slow growth in nitrogen oxide (NO_x) emissions and a continuous reduction after the year 2020 (Fig. S5), resulting in a decline of 6.4 ppb

(15.2%) in surface O_3 over eastern China by 1.5°C warming at 2060 (Fig. 3b). In contrast, RCP8.5 assumes fast growth of NO_x emissions with delayed controls after the year 2030, leading to surface O_3 enhancements of 6.6 ppb (15.7%) by 1.5°C warming at 2030. The lower emissions in RCP2.6 also result in smaller aerosol optical depth (AOD) than RCP8.5 (Fig. S6), leading to higher surface total radiation (Fig. 3c) while lower diffuse radiation (Fig. 3d) due to reducing light extinction (Yu et al., 2006).

3.2 Historical ecosystem productivity in China

The ensemble simulations show an increasing trend in GPP in China of 0.011 Pg C yr^{-2} over the historical period, 1901-2016 (Fig. 4a). A stronger trend of 0.022 Pg C yr^{-2} is found after 1960. Such change is much faster than the trend of 0.013 Pg C yr^{-2} estimated by a benchmark product (Jung et al., 2009) for 1982-2011 but close to a recent estimate of 0.02 Pg C yr^{-2} combining machine learning algorithms and eddy flux measurements from 40 sites in China (Yao et al., 2018). Simulated trend is also consistent with the TRENDY ensemble, which predicts trends of 0.013 ± 0.006 Pg C yr^{-2} (ensemble ± inter-model uncertainty) for 1901-2016 and 0.022 ± 0.01 Pg C yr^{-2} for 1961-2016. The YIBs simulations show variabilities of 0.41±0.23 Pg C yr^{-1} (6.2±3.9%, blue shading in Fig. 4a) due to uncertainties in climate from CMIP5 models, much smaller than the value of 1.33±0.16 Pg C yr^{-1} (19.2±2.6%, red shading in Fig. 4a) caused by structural uncertainties across different vegetation models.

NEE in China is negative, suggesting a regional land carbon sink (Fig. 4b). This sink is -94.7 Tg C yr^{-1} with a trend of -1.7 Tg C yr^{-2} during 1901-2016. Such change matches TRENDY simulations, which predict a multi-model mean carbon sink of -74.1±30.8 Tg C yr^{-1} (uncertainties due to inter-model variations) and a trend of -1.3±0.7 Tg C yr^{-2} for the same period. During 1980-1989, the ground-based estimate (Piao et al., 2009) suggests a sink of 177±73 Tg C yr^{-1} in China, consistent with the sink intensity of 149±20 Tg C yr^{-1} from the YIBs ensemble prediction. For the recent period of 1980-2000, YIBs estimates a strengthened sink of 154±30 Tg C yr^{-1} in China, weaker than the estimate of 198±114 Tg C yr^{-1} with the DLEM vegetation model (Tian et al., 2011)

but is within the estimates of 137-177 Tg C yr^{-1} based on both ground and satellite data (Fang et al., 2007). The interannual variability in YIBs simulations is much weaker than the estimates in other studies, because the ensemble approach largely dampen variations among different runs. Similar to GPP, the NEE simulations exhibit smaller variability of 62±50 Tg C yr^{-1} among different YIBs runs than that of 122±57 Tg C yr^{-1} among different TRENDY models.

3.3 Future changes of carbon fluxes

Projected GPP continues to increase in both RCP2.6 and RCP8.5 scenarios after the year 2016 (Fig. S7a). By the global warming of 1.5°C, GPP increases significantly in China, especially over eastern and northeastern parts (Fig. 5). Compared to the present day, GPP with O_3 effects increases by 1.07 ± 0.38 Pg C yr^{-1} (15.5 ± 5.4 %) in the RCP2.6 scenario (Fig. 5a) and 0.82 ± 0.30 Pg C yr^{-1} (11.9 ± 5.4%) in RCP8.5 (Fig. 5b). The spatial pattern of the GPP changes is similar in the two pathways (correlation coefficient R=0.93), except that ΔGPP in RCP2.6 is higher than in RCP8.5 by 30% with a positive center over eastern China (Fig. 5c). Projected NEE continues to be more negative in the RCP8.5 scenario after the year 2016 (Fig. S7b). Meanwhile, future NEE reaches the minimum value (or the maximum sink strength) around the year 2025 and then reverses to be less negative in the RCP2.6 scenario (Fig. S7b). By the period of 1.5°C global warming, NEE changes in China show opposite tendencies between the two pathways. Compared to the present day, NEE increases by 0.03 ± 0.03 Pg C yr^{-1} (-17.4±19.6 %) in RCP2.6 (Fig. 5d) but decreases by 0.14 ± 0.04 Pg C yr^{-1} (94.4±24.9 %) in RCP8.5 (Fig. 5e), suggesting that land carbon sink is slightly weakened in the former but strengthened in the latter. Their differences exhibit widespread positive values in China with high centers in the East (Fig. 5f).

The changes in carbon fluxes follow the variations in atmospheric composition and climate (Fig. 6 and Figs. S8-S11). By the global warming of 1.5°C, a dominant fraction of GPP enhancement in China is attributed to CO_2 fertilization (Fig. 6a). For the RCP2.6 scenario, CO_2 alone contributes 0.83 Pg C yr^{-1} (77%) to ΔGPP, with the highest

enhancement of 0.8 g C m^{-2} day^{-1} over the southeast coast (Fig. S8a). For RCP8.5, CO_2 fertilization increases GPP by 0.95 Pg C yr^{-1}, even higher than the total ΔGPP of 0.82 Pg C yr^{-1}. The larger CO_2-induced ΔGPP in RCP8.5 is due to the higher CO_2 concentrations (454 ppm) than RCP2.6 (442 ppm) at the same 1.5°C warming (Fig. 3a). The 12 ppm differences in CO_2 concentrations lead to a change of 0.12 Pg C yr^{-1} (1.7%) in GPP. This sensitivity of GPP to CO_2, 0.14% ppm^{-1}, falls within the range of 0.05-0.21% ppm^{-1} as predicted by 10 terrestrial models (Piao et al., 2013) and that of 0.01-0.32% ppm^{-1} as observed from multiple free-air CO_2 enrichment (FACE) sites (Ainsworth and Long, 2005). The higher ΔGPP in RCP2.6 instead yields a weakened NEE (more positive) due to the CO_2 effects (Fig. 6b). The stabilization of CO_2 concentrations in this scenario (Fig. 3a) results in a stabilized GPP after the year 2040 (Fig. S7a). Meanwhile, the 55-year (from 2005 to 2060) carbon accumulation enhances soil carbon storage by 10.5±1.3 Pg C and promotes soil respiration to 0.71±0.19 Pg C yr^{-1}. The stabilized GPP while enhanced soil respiration (NEE = Reco – GPP, Reco includes both soil and plant respiration) together lead to a weakened carbon sink (less negative NEE) by 1.5°C warming period (Fig. 7b). In contrast, soil carbon storage increases only 5.2±0.5 Pg C in RCP8.5 due to relatively short time period (from 2005 to 2031) for carbon accumulation, leading to lower soil respiration of 0.41±0.15 Pg C yr^{-1} in the fast warming pathway. The continuous increase of GPP and lower soil respiration jointly strengthen the land carbon sink (more negative NEE) in China by 0.1 Pg C yr^{-1} under RCP8.5 scenario (Fig. 6a).

Ozone (O_3) damages plant photosynthesis and the land carbon sink (Sitch et al., 2007;Yue and Unger, 2018). In the present day, O_3 decreases GPP by 6.7±2.6% (uncertainties ranging from low to high damaging sensitivities) in China (Fig. 7d), because of the direct inhibition of photosynthesis by 6±2.4% (Fig. 7a) and the consequent reduction of 1.8±0.8% in leaf area index (LAI, Fig. 7g). For 1.5°C global warming, this weakening effect shows opposite tendencies in the two RCP scenarios, with a reduced GPP loss of 4.7±2.0% in RCP2.6 (Fig. 7e) but an increased loss of 7.9±3.0% in RCP8.5 (Fig. 7f). These impacts are predominantly driven by the

variations of surface O_3 concentrations in the two scenarios, as predicted O_3 at 1.5°C warming decreases by 15.2% in the low emission pathway but increases by 15.7% in the high emission pathway (Fig. 3b). Consequently, changes in O_3 help increase GPP by 0.1±0.03 Pg C yr^{-1} in RCP2.6 but decrease GPP by 0.14±0.04 Pg C yr^{-1} in RCP8.5 for the same 1.5°C warming. Following the benefits to GPP, the lower O_3 decreases NEE (strengthens the sink) by 0.06±0.02 Pg C yr^{-1} in RCP2.6, offsetting more than half of the negative effect (weakens the sink) from CO_2 (Fig. 6b). For RCP8.5, O_3 impacts make limited contributions to ΔNEE.

Changes in meteorology account for the rest of the perturbations in the carbon fluxes. At the global warming of 1.5°C, temperature in China increases by 0.90°C for RCP2.6 and 0.91°C for RCP8.5 (Figs. S12a-S12b) compared to present-day climate. The spatial pattern of these changes is very similar without significant differences (Fig. S12c), leading to almost identical GPP responses (Figs. S8d and S9d). Generally, higher temperature is not beneficial for plant photosynthesis at low latitudes (Piao et al., 2013), where regional summer climate is already warmer than the optimal temperature threshold for leaf photosynthesis (Corlett, 2011). As a result, warming leads to negative changes in GPP over the East. Surface specific humidity exhibits widespread enhancement in eastern China (Figs. S13a-S13b). Air humidity may rise in a warmer climate because the corresponding enhancement of saturation pressure allows atmosphere to hold more water vapor. On average, surface specific humidity increases by 0.34 g kg^{-1} in RCP2.6 and 0.31 g kg^{-1} in RCP8.5, leading to a promotion of GPP by 0.14 Pg C yr^{-1} in the former and a similar value of 0.12 Pg C yr^{-1} in the latter (Figs. S8e and S9e). Precipitation increases by 0.14 mm day^{-1} (4.6%) over eastern China in RCP2.6 but decreases by 0.03 mm day^{-1} (1.2%) in RCP8.5 (Figs. S12d-S12e), leading to higher soil moisture in eastern China for RCP2.6 (Figs. S13d-S13e). Nevertheless, most of vegetation in eastern China is not water stressed, leaving moderate GPP responses to soil moisture changes in both RCP scenarios (Figs. S8f and S9f).

For the RCP2.6 scenario, the net effect of climate change causes an increase of 0.15 Pg

C yr^{-1} in GPP with a range from -0.54 to 0.62 Pg C yr^{-1} (Fig. 6a). Such large variability in ΔGPP is related to the uncertainties in meteorology from different climate models. For RCP8.5, climate-induced GPP change is only 0.04 Pg C yr^{-1} with a range from -0.6 to 0.26 Pg C yr^{-1}. The discrepancy of ΔGPP for the two pathways is mainly caused by the different radiation impacts, which enhance GPP by 0.2 Pg C yr^{-1} in RCP2.6 but only 0.11 Pg C yr^{-1} in RCP8.5 (Fig. 6a). Photosynthetically active radiation (PAR) is higher by 2.8 W m^{-2} in RCP2.6 than in RCP8.5 (Fig. 3c). The distinct changes in radiation are related to aerosol radiative effects, because global analyses also show radiation enhancement in regions (e.g., U.S. and Europe) with aerosol removal (Fig. S14). The lower AOD in RCP2.6 helps increase solar insolation at surface by reducing light extinction (Yu et al., 2006), and promote precipitation with weaker aerosol semi-direct and indirect effects (Lohmann and Feichter, 2005). Although lower aerosols in RCP2.6 slightly decrease diffuse radiation (Fig. 3d), which is more efficient in increasing photosynthesis (Mercado et al., 2009;Yue and Unger, 2018), the overall enhancement in total radiation helps boost GPP. Climate-induced ΔNEE is -0.02 Pg C yr^{-1} (strengthened sink) for both pathways (Fig. 6b), resulting from comparable responses of NEE to changes in radiation (R=0.82), temperature (R=0.71), air humidity (R=0.91), and soil moisture (R=0.73) between the two pathways (Figs. S10 and S11).

3.4 Impacts on allowable carbon budget

For a warming target of 1.5°C, our analyses suggest that a simultaneous reduction of CO_2 and air pollution emissions enhances the efficiency of land carbon uptake compared to a pathway without air pollution emission control. The increased light availability from aerosol removal and decreased surface O_3 jointly promote GPP in China by 0.3 Pg C yr^{-1}, equivalent to 36% of the CO_2 fertilization. In contrast, air pollution results in a net GPP inhibition of 0.03 Pg C yr^{-1} under the high emission pathway, suggesting a detrimental environment for plant health. Compared to RCP8.5, the timing of 1.5°C warming is delayed by 30 years in RCP2.6, leading to weaker carbon sink in the latter. However, even with the longer period of accumulation, the total carbon loss by O_3 damage is smaller by 3-16% in RCP2.6 relative to RCP8.5 at

the same warming level (Fig. 8a).

The slow warming increases the allowable cumulative anthropogenic carbon emissions. Assuming China's carbon emission fraction of 27% of the world (the level at year 2017) (Le Quere et al., 2018), the total national emissions allowed are 80.4 Pg C in RCP2.6 and 71.9 Pg C in RCP8.5 from the year 2010 to the 1.5°C warming, following the global emission rates defined for these scenarios. The ensemble simulations show that ecosystems in China help mitigate 8.5±1.1 Pg C in RCP2.6 and 4.5±0.6 Pg C in RCP8.5 (Fig. 8b). Sensitivity experiments with either reduced CO_2 (but retain high pollution) or reduced pollution (but retain high CO_2) reveal land carbon uptakes of 7.3±0.9 Pg C and 5.0±0.6 Pg C, respectively. These values are both lower than that in RCP2.6, suggesting that simultaneous control of carbon and air pollution emissions can maximize the mitigation potential of ecosystems. The higher ecosystem assimilation rate in a low emission pathway (10.6±1.4% in RCP2.6 vs. 6.3±0.8% in RCP8.5) over China, which is not considered in CMIP5 models, further buffers the pace to the global warming of 1.5°C.

4 Discussion and conclusions

Projection of future ecosystem productivity is subject to uncertainties in climate forcing and biophysical responses. The multi-model ensemble is a good approach to reduce the uncertainty in climate (Flato et al., 2013). In this study, we employ daily meteorology from 7 CMIP5 models. A comparison with more CMIP5 models is performed (not shown) and confirms that the changes in meteorology from the 7 selected climate models are robust and representative of future projections. As for ecosystem responses, future projections generally showed increasing GPP in China (Mu et al., 2008;Ji et al., 2008;Ju et al., 2007), however, climate change alone usually reduces productivity by inducing hot and drought weather conditions. In contrast, the YIBs simulations reveal a net positive effect of climate change on GPP though with large uncertainties (Fig. 6a). Such discrepancies are related to structural uncertainties across different vegetation models. Evaluations suggest that biophysical responses to environmental forcings in

the YIBs model are generally reasonable as compared to the TRENDY ensemble (Fig. 4).

The YIBs simulations do not consider nitrogen cycle and its limitation on carbon uptake. Inter-model comparisons show that models without nutrient constraints tend to overestimate GPP responses to CO_2 fertilization (Smith et al., 2016). As a result, the difference of CO_2 contributions in RCP scenarios would be smaller than predicted (Fig. 6a), suggesting that GPP enhancement in RCP2.6 might be even higher than RCP8.5 if nitrogen cycle is included. In contrast, nitrogen deposition in RCP2.6 would be much smaller than that in RCP8.5 due to emission control (Fig. S5), leading to lower nitrogen supply for ecosystem in the former scenario. Consequently, plant photosynthesis is confronted with stronger nutrient limit in RCP2.6 than that in RCP8.5, resulting in lower CO_2 fertilization efficiency in the former scenario. The net effect of nitrogen cycle on land carbon cycle is very uncertain (Zaehle et al., 2014;Huntzinger et al., 2017;Xiao et al., 2015).

For a warming target of 1.5°C, our analyses suggest that an associated reduction of CO_2 and pollution emissions brings more benefits to ecosystems in China than a pathway without emission control. The slow changes of temperature and other environmental variables due to slow growth of CO_2 are helpful for plant adaptation and limit biome shift (Warszawski et al., 2013), and the lower O_3 and higher solar radiation from aerosol removal increase plant photosynthesis. Consequently, China's ecosystems mitigate 10.6±1.4% of national emissions in the stabilized pathway, more efficient than the fraction of 6.3±0.8% in the transient pathway, leaving more allowable carbon budget for economic development and upgrade.

References

Ainsworth, E. A., and Long, S. P.: What have we learned from 15 years of free-air CO2 enrichment (FACE)? A meta-analytic review of the responses of photosynthesis, canopy, New Phytol, 165, 351-371, doi:10.1111/J.1469-8137.2004.01224.X, 2005.

Burke, M., Davis, W. M., and Diffenbaugh, N. S.: Large potential reduction in economic damages under UN mitigation targets, Nature, 557, 549-553, doi:10.1038/s41586-018-0071-9, 2018.

Clark, D. B., Mercado, L. M., Sitch, S., Jones, C. D., Gedney, N., Best, M. J., Pryor, M., Rooney, G. G., Essery, R. L. H., Blyth, E., Boucher, O., Harding, R. J., Huntingford, C., and Cox, P. M.: The Joint UK Land Environment Simulator (JULES), model description - Part 2: Carbon fluxes and vegetation dynamics, Geosci Model Dev, 4, 701-722, doi:10.5194/Gmd-4-701-2011, 2011.

Collins, W. J., Webber, C. P., Cox, P. M., Huntingford, C., Lowe, J., Sitch, S., Chadburn, S. E., Comyn-Platt, E., Harper, A. B., Hayman, G., and Powell, T.: Increased importance of methane reduction for a 1.5 degree target, Environ Res Lett, 13, 054003, doi:10.1088/1748-9326/aab89c, 2018.

Corlett, R. T.: Impacts of warming on tropical lowland rainforests, Trends Ecol Evol, 26, 606-613, doi:10.1016/j.tree.2011.06.015, 2011.

Dai, E. F., Wu, Z., Ge, Q. S., Xi, W. M., and Wang, X. F.: Predicting the responses of forest distribution and aboveground biomass to climate change under RCP scenarios in southern China, Global Change Biol, 22, 3642-3661, doi:10.1111/gcb.13307, 2016.

Defries, R. S., Hansen, M. C., Townshend, J. R. G., Janetos, A. C., and Loveland, T. R.: A new global 1-km dataset of percentage tree cover derived from remote sensing, Global Change Biol, 6, 247-254, doi:10.1046/J.1365-2486.2000.00296.X, 2000.

Fang, J. Y., Guo, Z. D., Piao, S. L., and Chen, A. P.: Terrestrial vegetation carbon sinks in China, 1981-2000, Sci China Ser D, 50, 1341-1350, doi:10.1007/s11430-007-0049-1, 2007.

Fang, J. Y., Shen, Z. H., Tang, Z. Y., Wang, X. P., Wang, Z. H., Feng, J. M., Liu, Y. N., Qiao, X. J., Wu, X. P., and Zheng, C. Y.: Forest community survey and the structural characteristics of forests in China, Ecography, 35, 1059-1071, doi:10.1111/j.1600-0587.2013.00161.x, 2012.

Farquhar, G. D., Caemmerer, S. V., and Berry, J. A.: A Biochemical-Model of Photosynthetic Co2 Assimilation in Leaves of C-3 Species, Planta, 149, 78-90, doi:10.1007/Bf00386231, 1980.

Flato, G., Marotzke, J., Abiodun, B., Braconnot, P., Chou, S. C., Collins, W., Cox, P., Driouech, F., Emori, S., Eyring, V., Forest, C., Gleckler, P., Guilyardi, E., Jakob, C., Kattsov, V., Reason, C., and Rummukainen, M.: Evaluation of Climate Models, in: Climate Change 2013: The Physical Science Basis. Contribution of Working Group I to the Fifth Assessment Report of the Intergovernmental Panel on Climate Change, edited by: Stocker, T. F., Qin, D., Plattner, G. K., Tignor, M., Allen, S. K., Boschung, J., Nauels, A., Xia, Y., Bex, V., and Midgley, P. M., Cambridge University Press, Cambridge, United Kingdom and New York, NY, USA, 2013.

Ghosh, A., Norton, B., and Duffy, A.: Effect of sky clearness index on transmission of evacuated (vacuum) glazing, Renewable Energy, 105, 160-166, doi:10.1016/j.renene.2016.12.056, 2017.

Hansen, M. C., DeFries, R. S., Townshend, J. R. G., Carroll, M., Dimiceli, C., and Sohlberg, R. A.: Global Percent Tree Cover at a Spatial Resolution of 500 Meters: First Results of the MODIS Vegetation Continuous Fields Algorithm, Earth Interact, 7, 1-15, doi:10.1175/1087-3562(2003)007<0001:GPTCAA>2.0.CO;2, 2003.

He, N. P., Wen, D., Zhu, J. X., Tang, X. L., Xu, L., Zhang, L., Hu, H. F., Huang, M., and Yu, G. R.: Vegetation carbon sequestration in Chinese forests from 2010 to 2050, Global Change Biol,

23, 1575-1584, doi:10.1111/gcb.13479, 2017.
Henley, B. J., and King, A. D.: Trajectories toward the 1.5 degrees C Paris target: Modulation by the Interdecadal Pacific Oscillation, Geophys Res Lett, 44, 4256-4262, doi:10.1002/2017gl073480, 2017.
Huntzinger, D. N., Michalak, A. M., Schwalm, C., Ciais, P., King, A. W., Fang, Y., Schaefer, K., Wei, Y., Cook, R. B., Fisher, J. B., Hayes, D., Huang, M., Ito, A., Jain, A. K., Lei, H., Lu, C., Maignan, F., Mao, J., Parazoo, N., Peng, S., Poulter, B., Ricciuto, D., Shi, X., Tian, H., Wang, W., Zeng, N., and Zhao, F.: Uncertainty in the response of terrestrial carbon sink to environmental drivers undermines carbon-climate feedback predictions, Scientific Reports, 7, 4765, doi:10.1038/s41598-017-03818-2, 2017.
James, R., Washington, R., Schleussner, C. F., Rogelj, J., and Conway, D.: Characterizing half-a-degree difference: a review of methods for identifying regional climate responses to global warming targets, Wires Clim Change, 8, e457, doi:10.1002/wcc.457, 2017.
Ji, J. J., Huang, M., and Li, K. R.: Prediction of carbon exchanges between China terrestrial ecosystem and atmosphere in 21st century, Sci China Ser D, 51, 885-898, doi:10.1007/s11430-008-0039-y, 2008.
Ju, W. M., Chen, J. M., Harvey, D., and Wang, S.: Future carbon balance of China's forests under climate change and increasing CO2, J Environ Manage, 85, 538-562, doi:10.1016/j.jenvman.2006.04.028, 2007.
Jung, M., Reichstein, M., and Bondeau, A.: Towards global empirical upscaling of FLUXNET eddy covariance observations: validation of a model tree ensemble approach using a biosphere model, Biogeosciences, 6, 2001-2013, doi:10.5194/bg-6-2001-2009, 2009.
Lam, J. C., and Li, D. H. W.: Correlation between global solar radiation and its direct and diffuse components, Build Environ, 31, 527-535, doi:10.1016/0360-1323(96)00026-1, 1996.
Lamarque, J. F., Shindell, D. T., Josse, B., Young, P. J., Cionni, I., Eyring, V., Bergmann, D., Cameron-Smith, P., Collins, W. J., Doherty, R., Dalsoren, S., Faluvegi, G., Folberth, G., Ghan, S. J., Horowitz, L. W., Lee, Y. H., MacKenzie, I. A., Nagashima, T., Naik, V., Plummer, D., Righi, M., Rumbold, S. T., Schulz, M., Skeie, R. B., Stevenson, D. S., Strode, S., Sudo, K., Szopa, S., Voulgarakis, A., and Zeng, G.: The Atmospheric Chemistry and Climate Model Intercomparison Project (ACCMIP): overview and description of models, simulations and climate diagnostics, Geosci Model Dev, 6, 179-206, doi:10.5194/gmd-6-179-2013, 2013.
Le Quere, C., Andrew, R. M., Friedlingstein, P., Sitch, S., Pongratz, J., Manning, A. C., Korsbakken, J. I., Peters, G. P., Canadell, J. G., Jackson, R. B., Boden, T. A., Tans, P. P., Andrews, O. D., Arora, V. K., Bakker, D. C. E., Barbero, L., Becker, M., Betts, R. A., Bopp, L., Chevallier, F., Chini, L. P., Ciais, P., Cosca, C. E., Cross, J., Currie, K., Gasser, T., Harris, I., Hauck, J., Haverd, V., Houghton, R. A., Hunt, C. W., Hurtt, G., Ilyina, T., Jain, A. K., Kato, E., Kautz, M., Keeling, R. F., Goldewijk, K. K., Kortzinger, A., Landschutzer, P., Lefevre, N., Lenton, A., Lienert, S., Lima, I., Lombardozzi, D., Metzl, N., Millero, F., Monteiro, P. M. S., Munro, D. R., Nabel, J. E. M. S., Nakaoka, S., Nojiri, Y., Padin, X. A., Peregon, A., Pfeil, B., Pierrot, D., Poulter, B., Rehder, G., Reimer, J., Rodenbeck, C., Schwinger, J., Seferian, R., Skjelvan, I., Stocker, B. D., Tian, H. Q., Tilbrook, B., Tubiello, F. N., van der Laan-Luijkx, I. T., van der Werf, G. R., van Heuven, S., Viovy, N., Vuichard, N., Walker, A. P., Watson, A. J., Wiltshire, A. J., Zaehle, S., and Zhu, D.: Global Carbon Budget 2017, Earth Syst Sci Data, 10, 405-448, doi:10.5194/essd-10-405-2018, 2018.

Lohmann, U., and Feichter, J.: Global indirect aerosol effects: a review, Atmospheric Chemistry and Physics, 5, 715-737, 2005.

Mann, M. E., Miller, S. K., Rahmstorf, S., Steinman, B. A., and Tingley, M.: Record temperature streak bears anthropogenic fingerprint, Geophys Res Lett, 44, 7936-7944, doi:10.1002/2017gl074056, 2017.

Meinshausen, M., Smith, S. J., Calvin, K., Daniel, J. S., Kainuma, M. L. T., Lamarque, J. F., Matsumoto, K., Montzka, S. A., Raper, S. C. B., Riahi, K., Thomson, A., Velders, G. J. M., and van Vuuren, D. P. P.: The RCP greenhouse gas concentrations and their extensions from 1765 to 2300, Climatic Change, 109, 213-241, doi:10.1007/S10584-011-0156-Z, 2011.

Mengis, N., Partanen, A.-I., Jalbert, J., and Matthews, H. D.: 1.5 °C carbon budget dependent on carbon cycle uncertainty and future non-CO2 forcing, Scientific Reports, 8, 5831, 2018.

Mercado, L. M., Bellouin, N., Sitch, S., Boucher, O., Huntingford, C., Wild, M., and Cox, P. M.: Impact of changes in diffuse radiation on the global land carbon sink, Nature, 458, 1014-U1087, doi:10.1038/Nature07949, 2009.

Millar, R. J., Fuglestvedt, J. S., Friedlingstein, P., Rogelj, J., Grubb, M. J., Matthews, H. D., Skeie, R. B., Forster, P. M., Frame, D. J., and Allen, A. R.: Emission budgets and pathways consistent with limiting warming to 1.5 degrees C, Nat Geosci, 10, 741-747, doi:10.1038/Ngeo3031, 2017.

Mitchell, D., Heaviside, C., Schaller, N., Allen, M., Ebi, K. L., Fischer, E. M., Gasparrini, A., Harrington, L., Kharin, V., Shiogama, H., Sillmann, J., Sippel, S., and Vardoulakis, S.: Extreme heat-related mortality avoided under Paris Agreement goals, Nat Clim Change, 8, 551-553, doi:10.1038/s41558-018-0210-1, 2018.

Mu, Q. Z., Zhao, M. S., Running, S. W., Liu, M. L., and Tian, H. Q.: Contribution of increasing CO(2) and climate change to the carbon cycle in China's ecosystems, J Geophys Res-Biogeo, 113, G01018, doi:10.1029/2006jg000316, 2008.

Nangombe, S., Zhou, T., Zhang, W., Wu, B., Hu, S., Zou, L., and Li, D.: Record-breaking climate extremes in Africa under stabilized 1.5°C and 2°C global warming scenarios, Nat Clim Change, 8, 375-380, doi:10.1038/s41558-018-0145-6, 2018.

Piao, S. L., Fang, J. Y., Ciais, P., Peylin, P., Huang, Y., Sitch, S., and Wang, T.: The carbon balance of terrestrial ecosystems in China, Nature, 458, 1009-U1082, doi:10.1038/nature07944, 2009.

Piao, S. L., Sitch, S., Ciais, P., Friedlingstein, P., Peylin, P., Wang, X. H., Ahlstrom, A., Anav, A., Canadell, J. G., Cong, N., Huntingford, C., Jung, M., Levis, S., Levy, P. E., Li, J. S., Lin, X., Lomas, M. R., Lu, M., Luo, Y. Q., Ma, Y. C., Myneni, R. B., Poulter, B., Sun, Z. Z., Wang, T., Viovy, N., Zaehle, S., and Zeng, N.: Evaluation of terrestrial carbon cycle models for their response to climate variability and to CO2 trends, Global Change Biol, 19, 2117-2132, doi:10.1111/Gcb.12187, 2013.

Rienecker, M. M., Suarez, M. J., Gelaro, R., Todling, R., Bacmeister, J., Liu, E., Bosilovich, M. G., Schubert, S. D., Takacs, L., Kim, G. K., Bloom, S., Chen, J. Y., Collins, D., Conaty, A., Da Silva, A., Gu, W., Joiner, J., Koster, R. D., Lucchesi, R., Molod, A., Owens, T., Pawson, S., Pegion, P., Redder, C. R., Reichle, R., Robertson, F. R., Ruddick, A. G., Sienkiewicz, M., and Woollen, J.: MERRA: NASA's Modern-Era Retrospective Analysis for Research and Applications, J Climate, 24, 3624-3648, doi:10.1175/Jcli-D-11-00015.1, 2011.

Schaefer, K., Collatz, G. J., Tans, P., Denning, A. S., Baker, I., Berry, J., Prihodko, L., Suits, N., and Philpott, A.: Combined Simple Biosphere/Carnegie-Ames-Stanford Approach terrestrial

carbon cycle model, J. Geophys. Res., 113, G03034, doi:10.1029/2007jg000603, 2008.
Schmidt, G. A., Kelley, M., Nazarenko, L., Ruedy, R., Russell, G. L., Aleinov, I., Bauer, M., Bauer, S. E., Bhat, M. K., Bleck, R., Canuto, V., Chen, Y. H., Cheng, Y., Clune, T. L., Del Genio, A., de Fainchtein, R., Faluvegi, G., Hansen, J. E., Healy, R. J., Kiang, N. Y., Koch, D., Lacis, A. A., LeGrande, A. N., Lerner, J., Lo, K. K., Matthews, E. E., Menon, S., Miller, R. L., Oinas, V., Oloso, A. O., Perlwitz, J. P., Puma, M. J., Putman, W. M., Rind, D., Romanou, A., Sato, M., Shindell, D. T., Sun, S., Syed, R. A., Tausnev, N., Tsigaridis, K., Unger, N., Voulgarakis, A., Yao, M. S., and Zhang, J. L.: Configuration and assessment of the GISS ModelE2 contributions to the CMIP5 archive, J Adv Model Earth Sy, 6, 141-184, doi:10.1002/2013ms000265, 2014.
Sitch, S., Cox, P. M., Collins, W. J., and Huntingford, C.: Indirect radiative forcing of climate change through ozone effects on the land-carbon sink, Nature, 448, 791-794, doi:10.1038/Nature06059, 2007.
Smith, W. K., Reed, S. C., Cleveland, C. C., Ballantyne, A. P., Anderegg, W. R. L., Wieder, W. R., Liu, Y. Y., and Running, S. W.: Large divergence of satellite and Earth system model estimates of global terrestrial CO2 fertilization, Nat Clim Change, 6, 306-310, doi:10.1038/Nclimate2879, 2016.
Solomon, S., Plattner, G.-K., Knutti, R., and Friedlingstein, P.: Irreversible climate change due to carbon dioxide emissions, P Natl Acad Sci USA, 106, 1704-1709, doi:10.1073/pnas.0812721106, 2009.
Spitters, C. J. T.: Separating the Diffuse and Direct Component of Global Radiation and Its Implications for Modeling Canopy Photosynthesis .2. Calculation of Canopy Photosynthesis, Agr Forest Meteorol, 38, 231-242, doi:10.1016/0168-1923(86)90061-4, 1986.
Stehfest, E., Zeist, W.-J. v., Valin, H., Havlik, P., Popp, A., Kyle, P., Tabeau, A., Mason-D'Croz, D., Hasegawa, T., Bodirsky, B. L., Calvin, K., Doelman, J. C., Fujimori, S., Humpenöder, F., Lotze-Campen, H., Meijl, H. v., and Wiebe, K.: Key determinants of global land-use projections, Nat Commun, 10, 2166, 2019.
Tian, H. Q., Xu, X. F., Lu, C. Q., Liu, M. L., Ren, W., Chen, G. S., Melillo, J., and Liu, J. Y.: Net exchanges of CO2, CH4, and N2O between China's terrestrial ecosystems and the atmosphere and their contributions to global climate warming, Journal of Geophysical Research, 116, G02011, doi:10.1029/2010jg001393, 2011.
Warszawski, L., Friend, A., Ostberg, S., Frieler, K., Lucht, W., Schaphoff, S., Beerling, D., Cadule, P., Ciais, P., Clark, D. B., Kahana, R., Ito, A., Keribin, R., Kleidon, A., Lomas, M., Nishina, K., Pavlick, R., Rademacher, T. T., Buechner, M., Piontek, F., Schewe, J., Serdeczny, O., and Schellnhuber, H. J.: A multi-model analysis of risk of ecosystem shifts under climate change, Environ Res Lett, 8, 044018, doi:10.1088/1748-9326/8/4/044018, 2013.
Weedon, G. P., Balsamo, G., Bellouin, N., Gomes, S., Best, M. J., and Viterbo, P.: The WFDEI meteorological forcing data set: WATCH Forcing Data methodology applied to ERA-Interim reanalysis data, Water Resources Research, 50, 7505-7514, doi:10.1002/2014wr015638, 2014.
Wu, S., Yin, Y., Zhao, D., Huang, M., Shao, X., and Dai, E.: Impact of future climate change on terrestrial ecosystems in China, International Journal of Climatology, 30, 866-873, doi:10.1002/joc.1938, 2009.
Xiao, J. F., Zhou, Y., and Zhang, L.: Contributions of natural and human factors to increases in vegetation productivity in China, Ecosphere, 6, 233, doi:10.1890/Es14-00394.1, 2015.
Yao, Y. T., Wang, X. H., Li, Y., Wang, T., Shen, M. G., Du, M. Y., He, H. L., Li, Y. N., Luo, W. J.,

Ma, M. G., Ma, Y. M., Tang, Y. H., Wang, H. M., Zhang, X. Z., Zhang, Y. P., Zhao, L., Zhou, G. S., and Piao, S. L.: Spatiotemporal pattern of gross primary productivity and its covariation with climate in China over the last thirty years, Global Change Biol, 24, 184-196, doi:10.1111/gcb.13830, 2018.

Yu, H., Kaufman, Y. J., Chin, M., Feingold, G., Remer, L. A., Anderson, T. L., Balkanski, Y., Bellouin, N., Boucher, O., Christopher, S., DeCola, P., Kahn, R., Koch, D., Loeb, N., Reddy, M. S., Schulz, M., Takemura, T., and Zhou, M.: A review of measurement-based assessments of the aerosol direct radiative effect and forcing, Atmos. Chem. Phys., 6, 613-666, 2006.

Yue, X., and Unger, N.: The Yale Interactive terrestrial Biosphere model: description, evaluation and implementation into NASA GISS ModelE2, Geosci Model Dev, 8, 2399-2417, doi:10.5194/gmd-8-2399-2015, 2015.

Yue, X., and Unger, N.: Aerosol optical depth thresholds as a tool to assess diffuse radiation fertilization of the land carbon uptake in China, Atmospheric Chemistry and Physics, 17, 1329-1342, doi:10.5194/acp-17-1329-2017, 2017.

Yue, X., Unger, N., Harper, K., Xia, X., Liao, H., Zhu, T., Xiao, J., Feng, Z., and Li, J.: Ozone and haze pollution weakens net primary productivity in China, Atmospheric Chemistry and Physics, 17, 6073-6089, doi:10.5194/acp-17-6073-2017, 2017.

Yue, X., and Unger, N.: Fire air pollution reduces global terrestrial productivity, Nat Commun, 9, 5413, doi:10.1038/s41467-018-07921-4, 2018.

Zaehle, S., Medlyn, B. E., De Kauwe, M. G., Walker, A. P., Dietze, M. C., Hickler, T., Luo, Y. Q., Wang, Y. P., El-Masri, B., Thornton, P., Jain, A., Wang, S. S., Warlind, D., Weng, E. S., Parton, W., Iversen, C. M., Gallet-Budynek, A., McCarthy, H., Finzi, A. C., Hanson, P. J., Prentice, I. C., Oren, R., and Norby, R. J.: Evaluation of 11 terrestrial carbon-nitrogen cycle models against observations from two temperate Free-Air CO2 Enrichment studies, New Phytol, 202, 803-822, doi:10.1111/Nph.12697, 2014.

Author Contributions

X.Y., H.L., and H.W. designed the research and wrote the manuscript. X.Y. downloaded CMIP5 data, set up models, and performed all simulations. T.Z. evaluated diffuse radiation models. N.U. provided ACCMIP data. S.S. provided TRENDY data. Z.F. provided O_3 damaging meta-analysis data in China. J.Y. analyzed TRENDY results over China. All authors contributed to the interpretation of the results and improvement of the paper.

Acknowledgements

This work is supported by the National Key Research and Development Program of China (grant no. 2017YFA0603802) and National Natural Science Foundation of China (grant no. 91744311, 41975155).

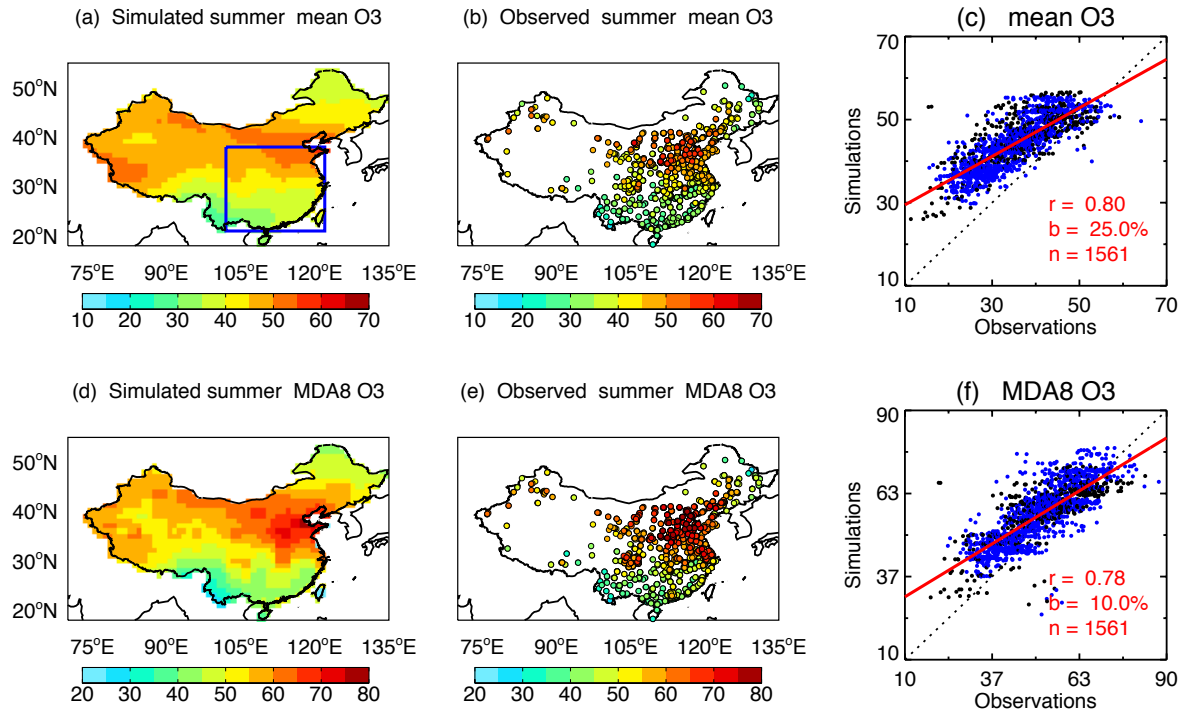

Figure 1. Evaluation of surface O_3 with site-level observations. Simulations are ensemble (a) mean and (d) daily maximum 8-hour average (MDA8) O_3 for the period of 2005-2015 from 12 ACCMIP models. Observations (b and e) are the average during 2015-2018 from 1580 sites operated by Ministry of Ecology and Environment, China. The correlation coefficients (r), relative biases (b), and number of sites (n, excluding data-missing sites) are shown in the scatter plots (c and f). The blue points in the scatter plots represent sites located within the box regions in eastern China as shown in (a). The dashed line represents the 1:1 ratio. The red line is the linear regression between simulations and observations.

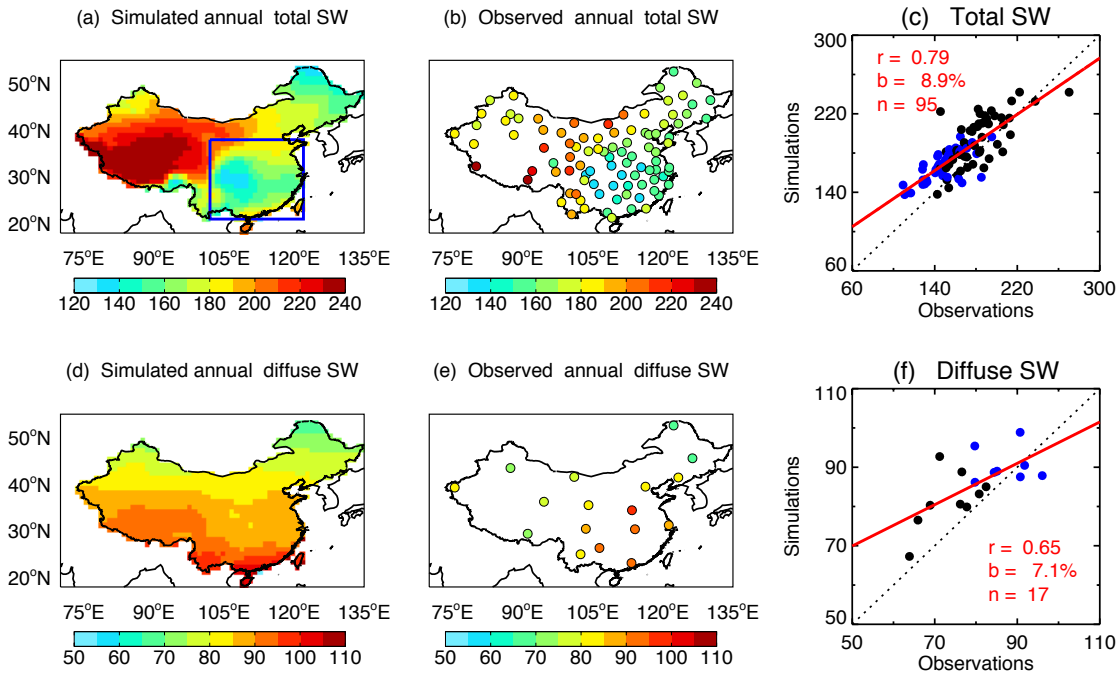

Figure 2. Evaluation of radiation fluxes with site-level observations. Simulations are surface (a) total shortwave radiation (W m^{-2}) and (d) diffuse radiation derived with method M01 (Table S4) for the period of 2005-2015 from an ensemble of 7 CMIP5 climate models. Observations (b and e) are the average during 2009-2011 from 106 sites operated by the Climate Data Center, Chinese Meteorological Administration. The correlation coefficients (r), relative biases (b), and number of sites (n, excluding data-missing sites) are shown in the scatter plots (c and f). The blue points in the scatter plots represent sites located within the box regions in eastern China as shown in (a). The dashed line represents the 1:1 ratio. The red line is the linear regression between simulations and observations.

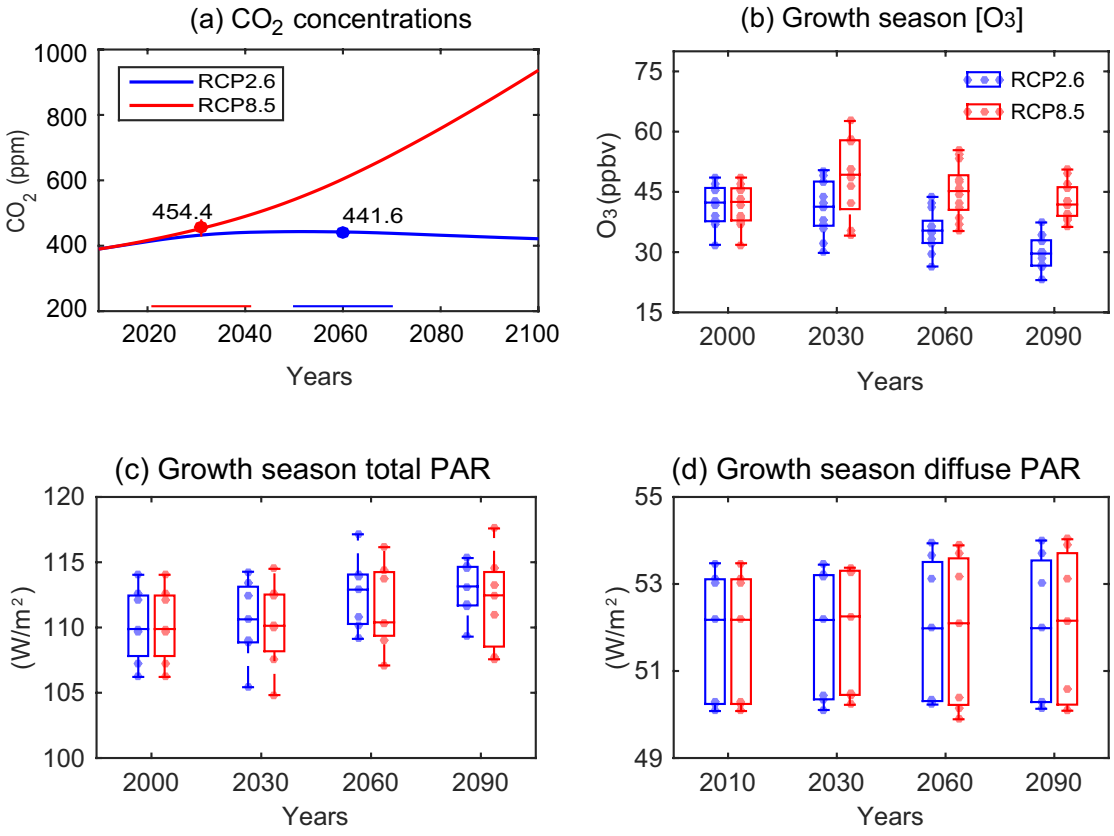

Figure 3. Changes in atmospheric compositions and radiation. Results shown are projected future (a) global CO_2 concentrations, and (b) surface O_3 concentrations, (c) total Photosynthetically Active Radiation (PAR), and (d) diffuse PAR at growth season in China. The average (a) CO_2 concentrations at the global warming of 1.5°C are 442 ppm for RCP2.6 scenario (blue, 2050-2070) and 454 ppm for RCP8.5 scenario (red, 2021-2041). The (b) O_3 concentrations are averaged over east of 110ºE in China from 12 ACCMIP models for RCP2.6 (blue) and RCP8.5 (red) scenarios. Each dot represents the value averaged for May to September from a chemistry model. The (c-d) PAR values are averaged over China from 7 CMIP5 models for RCP2.6 (blue) and RCP8.5 (red) scenarios. Diffuse PAR is calculated using hourly total PAR and solar zenith angle based on the parameterization M01. Each dot represents the value averaged for May to September from a climate model. For each selected year in (b-d), a period of 11 years (5 years before and 5 years after) is used to derive the decadal mean values.

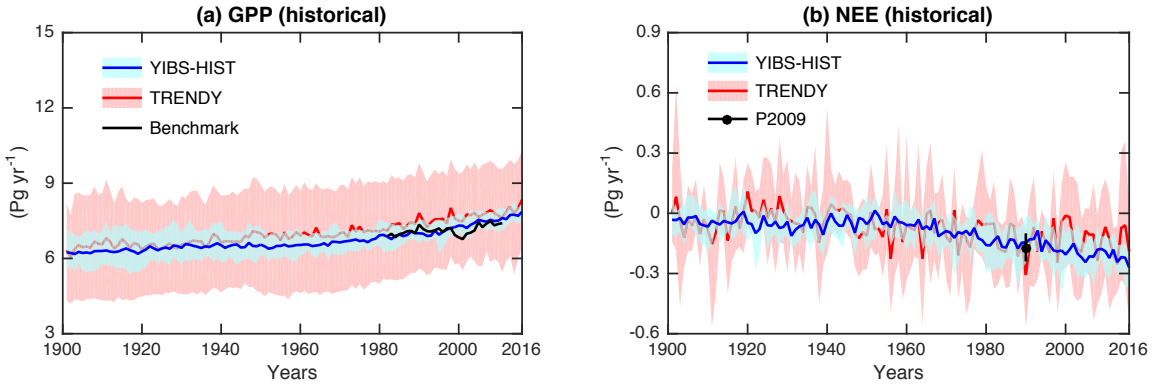

Figure 4. Historical carbon fluxes in China. Results shown are simulated (a) gross primary productivity (GPP) and (b) net ecosystem exchange (NEE) during historical period (1901-2016) using YIBs model (blue), and the comparison with predictions of 14 terrestrial models from TRENDY project (red). The bold lines are ensemble means with red shadings for inter-vegetation-model uncertainties and blue shadings for inter-climate-model uncertainties. All YIBs simulations are driven with daily meteorology from CMIP5 models. All TRENDY simulations are driven with CRUNCEP meteorology. The black line in (a) represents benchmark results of 1980-2011 from Jung et al. (2009). The black point with error bar in (b) represents the synthesis of ground- and model-based estimate of NEE in China by Piao et al. (2009).

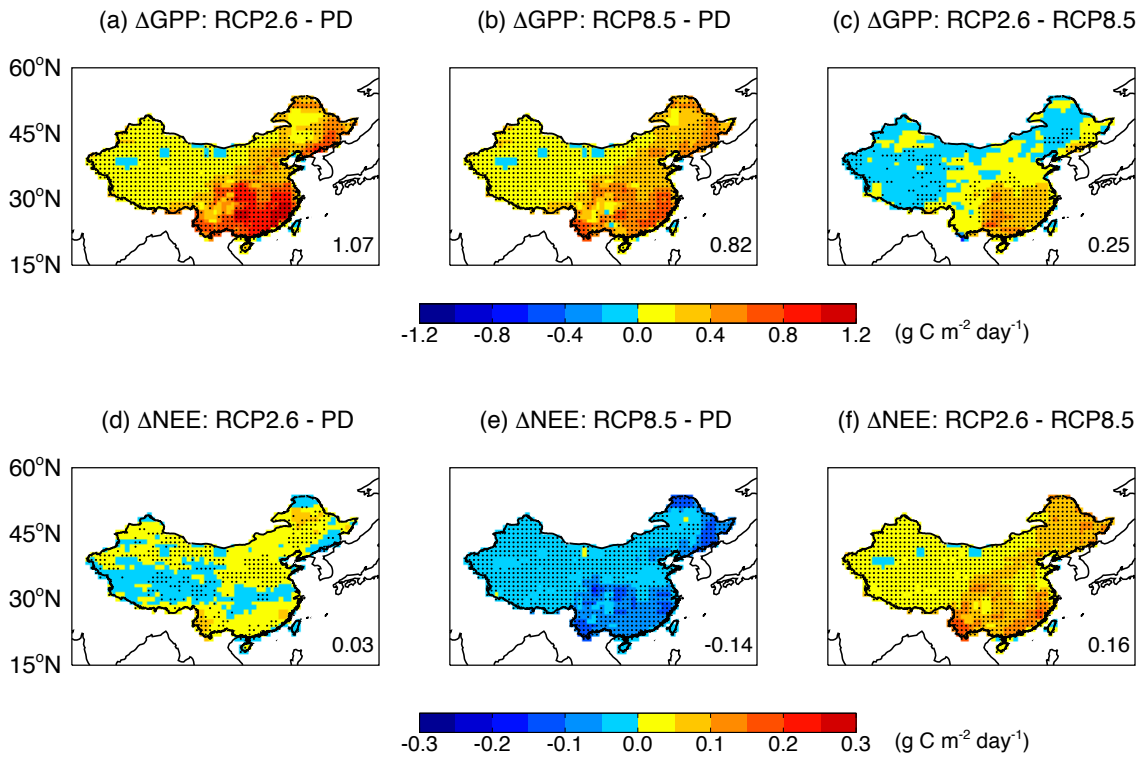

Figure 5. Changes in carbon fluxes by global warming of 1.5ºC. Results shown are simulated (top) GPP and (bottom) NEE over China between the period of global warming of 1.5ºC and present day (1995-2015) under (left) RCP2.6 scenario, (middle) RCP8.5 scenario, and (right) their differences. The period of global warming of 1.5 ºC is set to 2050-2070 for RCP2.6 and 2021-2041 for RCP8.5. Simulations are performed using YIBs vegetation model driven with daily meteorology from 7 CMIP5 models. The O_3 damaging effect is included with predicted ensemble O_3 concentrations from 12 ACCMIP models. For each grid, significant changes at $p<0.05$ are marked with dots. The total changes (Pg C yr^{-1}) over China are shown in each panel.

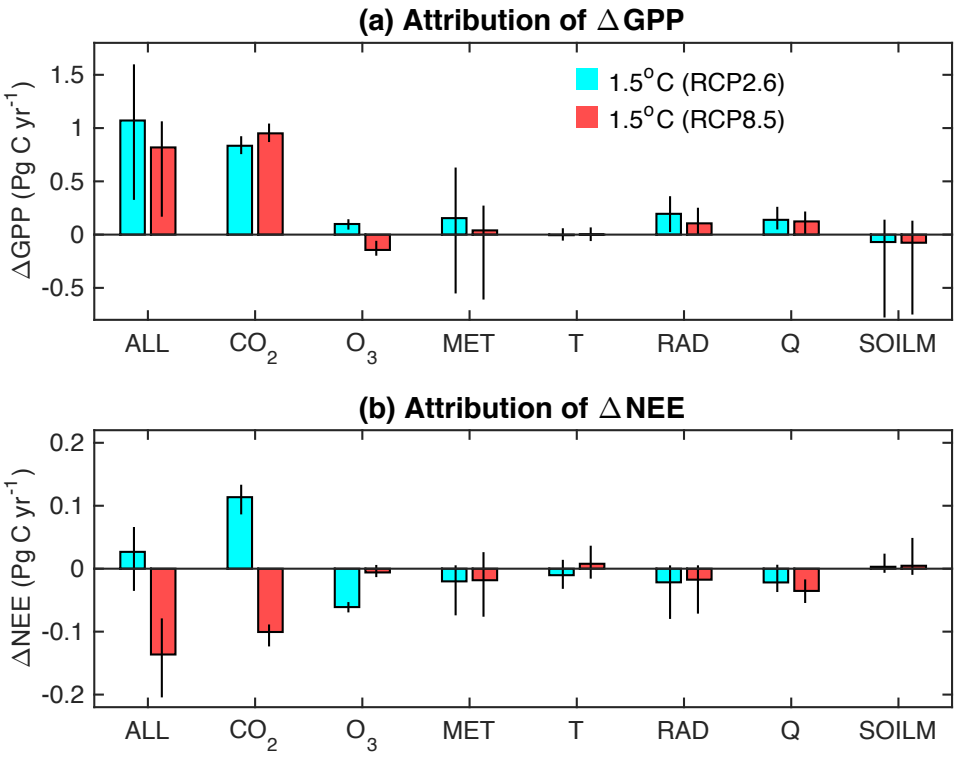

Figure 6. Attribution of changes in GPP and NEE to individual driving factors. Results shown are the predicted GPP changes in China between the period of global warming of 1.5ºC and present day (1995-2015) caused by all (ALL) or individual driving factors, including CO_2 fertilization, O_3 damaging, and meteorological changes (MET). The perturbations by meteorology is a combination of those by temperature (T), radiation (RAD), specific humidity (Q), and soil moisture (SOILM). The contrast is shown between the scenarios of RCP2.6 (blue, 2050-2070) and RCP8.5 (red, 2021-2041). The error bars indicate uncertainties of YIBs simulations using different future meteorology from 7 CMIP5 models.

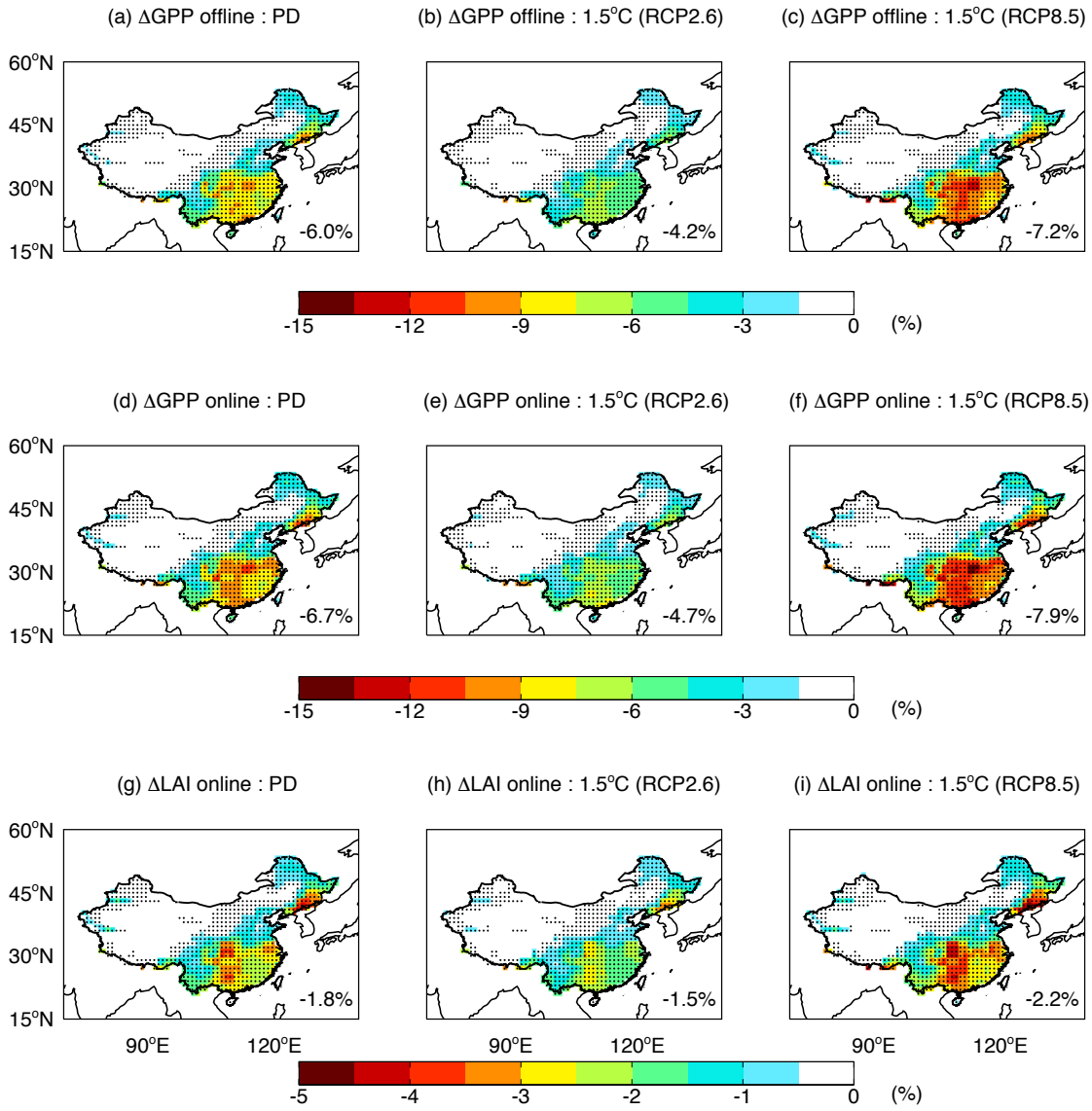

Figure 7. Damaging effects of O_3 to photosynthesis and plant growth. Results shown are ensemble mean changes in (top) offline GPP, (middle) online GPP, and (bottom) leaf area index (LAI) caused by O_3 at (left) present day (1995-2015) and 1.5°C warming under (middle) RCP.6 (2050-2070) and (right) RCP8.5 (2021-2041) scenarios. The simulations are performed with YIBs vegetation model driven with meteorology from 7 CMIP5 models and hourly ozone derived from 12 ACCMIP models. The damaging effect is averaged for high and low O_3 sensitivities. For each grid, significant changes at $p<0.05$ are marked with dots. The mean changes over China are shown in each panel.

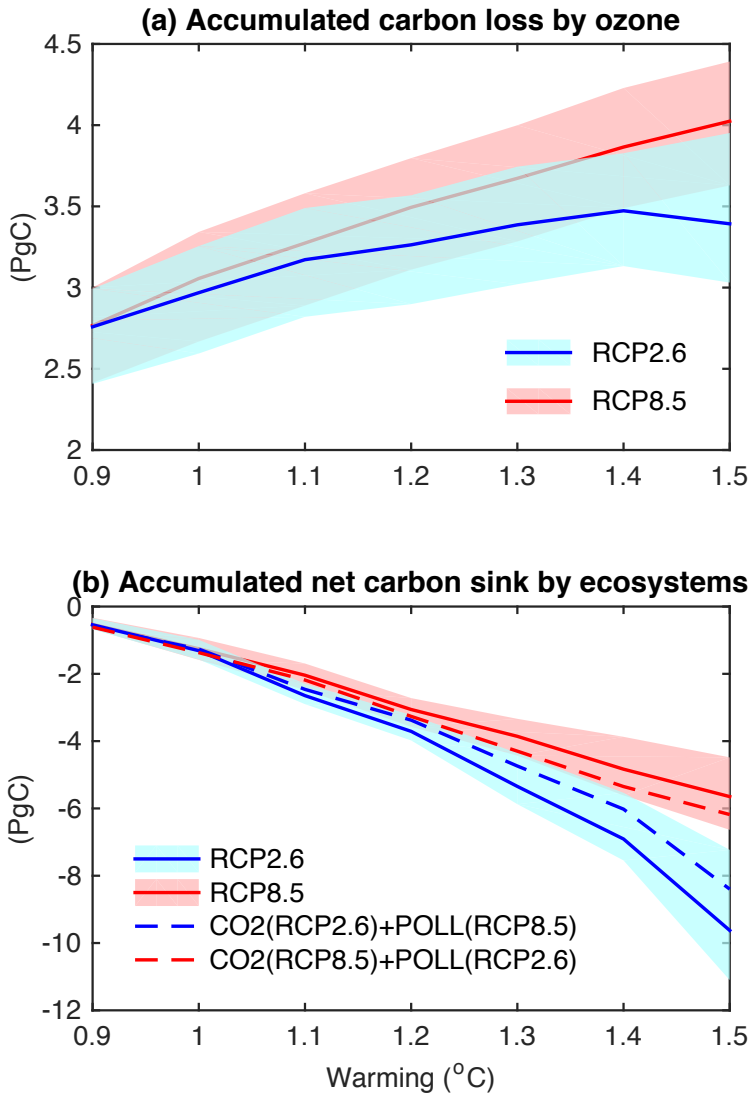

Figure 8. Accumulated carbon budget in China by 1.5ºC global warming. The top panel shows the total carbon loss of ecosystems caused by O_3 damaging effects at different warming thresholds for two emission pathways. The bottom panel shows the accumulated net carbon sink by ecosystems in China at the 1.5ºC global warming. The two solid lines represent emissions of CO_2 and pollutants from the same scenario, either RCP2.6 (blue) or RCP8.5 (red). The dashed lines represent sensitivity experiments with inconsistent CO_2 and pollutants, with the blue (red) line driven with CO_2 from RCP2.6 (RCP8.5) but air pollution from RCP8.5 (RCP2.6). The warming of 1.0 ºC is the year 2010 for both RCP2.6 and RCP8.5 scenarios.